


# Revisit of the anisotropic vortex states of 2H-$NbSe_2$ towards the zero-field limit

Fan Zhang(张凡), Xingyuan Hou(侯兴元), Yuxuan Jiang(姜宇轩), Zongyuan Zhang(张宗源), Yubing Tu(涂玉兵), Xiangde Zhu(朱相德), Genfu Chen(陈根富), and Lei Shan(单磊)

**Citation:**Chin. Phys. B, 2024, 33 (**6**): 067401. DOI: 10.1088/1674-1056/ad362d
Journal homepage: http://cpb.iphy.ac.cn; http://iopscience.iop.org/cpb

**What follows is a list of articles you may be interested in**

---

## Dynamic vortex Mott transition in triangular superconducting arrays

Zi-Xi Pei(裴子玺), Wei-Gui Guo(郭伟贵), and Xiang-Gang Qiu(邱祥冈)
Chin. Phys. B, 2022, 31 (**3**): 037404. DOI: 10.1088/1674-1056/ac3cb1

## Electronic properties and interfacial coupling in Pb islands on single-crystalline graphene

Jing-Peng Song(宋靖鹏) and Ang Li(李昂)
Chin. Phys. B, 2022, 31 (**3**): 037401. DOI: 10.1088/1674-1056/ac1b8e

## Evidence for topological superconductivity: Topological edge states in $Bi_2Te_3$/FeTe heterostructure

Bin Guo(郭斌), Kai-Ge Shi(师凯歌), Hai-Lang Qin(秦海浪), Liang Zhou(周良), Wei-Qiang Chen(陈伟强), Fei Ye(叶飞), Jia-Wei Mei(梅佳伟), Hong-Tao He(何洪涛), Tian-Luo Pan(潘天洛), Gan Wang(王干)
Chin. Phys. B, 2020, 29 (**9**): 097403. DOI: 10.1088/1674-1056/abaf9c

## Electronic structure and spatial inhomogeneity of iron-based superconductor FeS

Chengwei Wang(王成玮), Meixiao Wang(王美晓), Juan Jiang(姜娟), Haifeng Yang(杨海峰), Lexian Yang(杨乐仙), Wujun Shi(史武军), Xiaofang Lai(赖晓芳), Sung-Kwan Mo, Alexei Barinov, Binghai Yan(颜丙海), Zhi Liu(刘志), Fuqiang Huang(黄富强), Jinfeng Jia(贾金峰), Zhongkai Liu(柳仲楷), Yulin Chen(陈宇林)
Chin. Phys. B, 2020, 29 (**4**): 047401. DOI: 10.1088/1674-1056/ab75d4

## Surface Majorana flat bands in $j$=3/2 superconductors with singlet-quintet mixing

Jiabin Yu(于家斌), Chao-Xing Liu(刘朝星)
Chin. Phys. B, 2020, 29 (**1**): 017402. DOI: 10.1088/1674-1056/ab5b89

---

**RAPID COMMUNICATION**

# Revisit of the anisotropic vortex states of 2H-$NbSe_2$ towards the zero-field limit

Fan Zhang(张凡)[1,2], Xingyuan Hou(侯兴元)[3,4,5,†], Yuxuan Jiang(姜宇轩)[6,3,‡], Zongyuan Zhang(张宗源)[4,5], Yubing Tu(涂玉兵)[4,5], Xiangde Zhu(朱相德)[7], Genfu Chen(陈根富)[1,2], and Lei Shan(单磊)[3,4,5,8,§]

[1] *Beijing National Laboratory for Condensed Matter Physics, Institute of Physics, Chinese Academy of Sciences, Beijing* 100190, *China*
[2] *School of Physical Sciences, University of Chinese Academy of Sciences, Beijing* 100190, *China*
[3] *Center of Free Electron Laser and High Magnetic Field, Anhui University, Hefei* 230601, *China*
[4] *Information Materials and Intelligent Sensing Laboratory of Anhui Province, Institutes of Physical Science and Information Technology, Anhui University, Hefei* 230601, *China*
[5] *Key Laboratory of Structure and Functional Regulation of Hybrid Materials in Anhui University, Ministry of Education, Hefei* 230601, *China*
[6] *School of Physics and Materials Science, Anhui University, Hefei* 230601, *China*
[7] *Anhui Key Laboratory of Condensed Matter Physics at Extreme Conditions, High Magnetic Field Laboratory, HFIPS, Anhui, Chinese Academy of Sciences, and University of Science and Technology of China, Hefei* 230031, *China*
[8] *Hefei National Laboratory, Hefei* 230088, *China*

(Received 18 February 2024; revised manuscript received 11 March 2024; accepted manuscript online 21 March 2024)

We revisited the vortex states of 2H-$NbSe_2$ towards zero fields by a low-temperature scanning tunneling microscope. Fine structures of the anisotropic vortex states were distinguished, one is a spatially non-splitting zero bias peak, and the other is an in-gap conductance anomaly resembling evolved crossing features around the center of the three nearest vortices. Both of them distribute solely along the next nearest neighboring direction of the vortex lattice and become unresolved in much higher magnetic fields, implying an important role played by the vortex–vortex interactions. To clarify these issues, we have studied the intrinsic vortex states of the isolated trapped vortex in zero fields at 0.45 K. It is concluded that the anisotropic zero bias peak is attributed to the superconducting gap anisotropy, and the spatially evolved crossing features are related to the vortex–vortex interaction. The vortex core size under the zero-field limit is determined. These results provide a paradigm for studying the inherent vortex states of type-Ⅱ superconductors especially based on an isolated vortex.

**Keywords:** vortex states, zero-bias conductance peak, scanning tunneling microscopy

**PACS:** 74.25.Ha, 74.55.+v, 47.32.cb **DOI:** 10.1088/1674-1056/ad362d

## 1. Introduction

It has been well-known that arrayed magnetic vortices carrying quantized flux $\phi_0$ form in a type-Ⅱ superconductor between the lower and upper critical magnetic fields.[1] Centered around each vortex, the field maintained by the surrounding superfluid decays on the length scale of the penetration depth $\lambda$, and the order parameter $\Delta(\boldsymbol{r})$ recovers from zero to its asymptotic value on another length scale of the coherence length $\xi$.[2] It is predicted that the spatially confined quasiparticles lie in the discrete levels with the energies of $\mu\Delta^2/E_{\rm F}$ ($\mu = \pm 1/2, \pm 3/2, \ldots$) in s-wave superconductors.[3–5] The study of vortex bound states has long been an attractive topic for the close correlation to the superconducting order parameters and the pairing mechanism. Moreover, it has been found that an additional half-integer level shift produces the robust Majorana zero modes (MZMs) in the topological vortices.[6–16] These fine electronic structures could be directly visualized by the scanning tunneling microscope/spectroscopy (STM/STS) for the ability to map the local density of states (LDOS) on the atomic scale.[17–21] By tracing the spatial dependence of the LDOS, the evolution of the vortex bound states could be unveiled, which also helps to identify the MZMs in the topological vortices.

However, the superfluid around a vortex could overlap with each other in finite fields since the $\lambda$ is much larger than $\xi$. Firstly, the reduction in vortex core size caused by the cancellation of the opposite supercurrent surrounding the adjacent vortices, which is defined as the vortex lattice squeezing effect, could significantly modify the distribution of $\boldsymbol{j}_{\rm s}(\boldsymbol{r})$, and thus $B(\boldsymbol{r})$ and $\Delta(\boldsymbol{r})$.[22,23] Secondly, as the magnetic field further increases, the bound state wavefunctions of the neighboring vortices will undergo hybridization, enabling the intervortex transfer of the quasiparticles.[24–26] These effects of vortex–vortex interactions have a giant influence on the identification of the vortex bound states. For example, the probability of MZMs in vortex cores of the candidate topological superconductors could decrease in higher fields due to the vortex–vortex interactions.[27] Most recently, a spatially non-splitting

†Corresponding author. E-mail: xyhou@ahu.edu.cn
‡Corresponding author. E-mail: yuxuan.jiang@ahu.edu.cn
§Corresponding author. E-mail: lshan@ahu.edu.cn

© 2024 Chinese Physical Society and IOP Publishing Ltd 

zero-bias conductance peak (ZBCP) was observed in a normal superconductor La in a low field, which was attributed to the anisotropy of its Fermi surface (FS).[28] In fact, theoretical works indicate that similar non-splitting ZBCP could also exist in the vortices of an s-wave superconductor with significantly anisotropic superconducting order parameters.[29,30] These results raised doubt on the explanation of the non-splitting ZBCP in vortex cores by MZMs in superconductors far from the quantum limit. As the most favored platform to study the trivial vortex states, 2H-$NbSe_2$ (next abbreviated as $NbSe_2$) possesses anisotropic order parameters as revealed by the angle-resolved photoemission spectroscopy (ARPES) measurements,[31] and exhibits spatially anisotropic vortex bound states.[32] Therefore, intrinsic vortex structures excluding vortex–vortex interactions are valuable to be studied in this archetypical system, in particular for an isolated vortex at the zero-field limit.

In this paper, we report a close inspection of the anisotropic vortex states of $NbSe_2$ single crystals especially under the extremely low magnetic fields and the zero-field limit by using a low-temperature STM. Fine structures of electronic states were revealed with a legible spatial evolution, which could not be well distinguished at much higher magnetic fields. One is an anisotropic non-splitting ZBCP that still exists until the zero-field limit, which could be ascribed to the anisotropy of the superconducting gap, in good agreement with a simulation based on quasi-classical theory. Another is an in-gap conductance anomaly resembling evolved crossing features around the center of the three nearest vortices, which originates from vortex–vortex interactions. Furthermore, the field-dependent vortex core size including zero-field vortex core size could be determined. These results provide a paradigm for studying the intrinsic properties of type-Ⅱ superconductors based on an isolated vortex.

## 2. Experimental details

High quality $NbSe_2$ single crystals of clean limit studied were grown by the chemical vapor transport method with slightly excess selenide as the transport agent.[33] The transition temperature was about 7.1 K determined by the resistivity measurement. STM/STS measurements were carried out on a commercial facility (USM1300, Unisoku Co., Ltd.). The samples were mechanically cleaved in an ultrahigh vacuum (UHV) environment and then transferred immediately into the STM head maintained at a low temperature. Electrochemically etched tungsten tips were used after *in situ* treatment and calibration on Au(111) film. The topographic images were acquired in the constant-current mode with a bias voltage applied to the sample. The tunneling spectra of $\mathrm{d}I/\mathrm{d}V \sim V$ were obtained using the standard lock-in technique at 973.137 Hz. Most spectroscopic measurements were carried out at 0.45 K unless otherwise specified.

## 3. Results and discussion

Figure 1(a) shows an atomically resolved topography of $NbSe_2$ with the modulations of the incommensurate charge density waves. The primary vectors of the hexagonal lattice are labeled by the two arrows $a$ and $b$. At the temperature of 0.45 K far below the $T_c$, the system entirely enters the superconducting state with the prominent gap dominating the tunneling spectrum represented by the black curve in the inset of Fig. 1(a). After applying a magnetic field of 200 mT, a broad ZBCP feature shows up at the vortex center due to the small energy interval $\Delta^2/E_F$ of the formed vortex bound states, as denoted by the red curve in the inset.[3] Thus, we can identify the spatially distributed vortices by imaging the conductance map of $\mathrm{d}I/\mathrm{d}V$ ($\boldsymbol{r}, E = 0$ meV) as shown in Fig. 1(b). They arrange into a hexagonal lattice with the field-dependent period of $L = (2\phi_0/(\sqrt{3}B))^{1/2}$, with the intervortex spacing approximately 109 nm at 200 mT. The nearest neighboring direction labeled as $\theta_1$ is exactly the same as the Se–Se directions. The LDOS around each vortex center shows a star-shaped modulation, with six rays extending from the vortex center along the next nearest neighboring direction labeled as $\theta_2$, and it also confirms that the sample is at the clean limit.

Then we studied the evolutions of the LDOS along $\theta_1$ and $\theta_2$ at 0.45 K under different magnetic fields to reveal the anisotropic properties of the vortex states. For convenience to the comparison, the trajectories are normalized by the corresponding intervortex spacing $L$. Along the direction of $\theta_1$ shown in the false-color images of Figs. 1(c)–1(h), the established ZBCP at the vortex center splits into symmetric dispersive branches indicated by the dashed lines, which results from the quasiparticles wave function extending into a larger radius at higher energy. Notably, the branches indicated by the grey dashed lines become visible below 200 mT and consistently extend to $L/2$, while the extension length of the outer branch has a relatively weak field dependence estimated from the LDOS evolutions as indicated by the orange line segments. Along the direction of $\theta_2$ shown in Figs. 1(i)–1(n), two pairs of dispersive branches are also resolved under 200 mT as indicated by the black and grey dashed lines, respectively. Besides, another two subtle in-gap features are also identified, which are absent on the spectra along $\theta_1$. The first one is the conductance enhancement near the center of the three nearest vortices indicated by the red arrows. At the low fields under 200 mT, they become much clearer to be resolved as two gradually approaching X-shaped crossings. These crossing features are rarely noticed in earlier literature. The other feature is an emergent ZBCP as indicated by the red dash line.

Without splitting in our resolution, it nearly extends to the location where the X-shaped crossings appear. These two zero-bias anomalies along $\theta_2$ seem to contribute to the six rays of the star-shaped vortex states together. Whereas, a spatially non-splitting ZBCP in vortex cores is always interpreted as an essential signature of MZMs in several topological superconductor candidates.[10–16] Thus, the observation is particularly abnormal for the topologically trivial electronic structure of $NbSe_2$, and it will be instructive to further visualize these fine anisotropic features in this archetypical system.

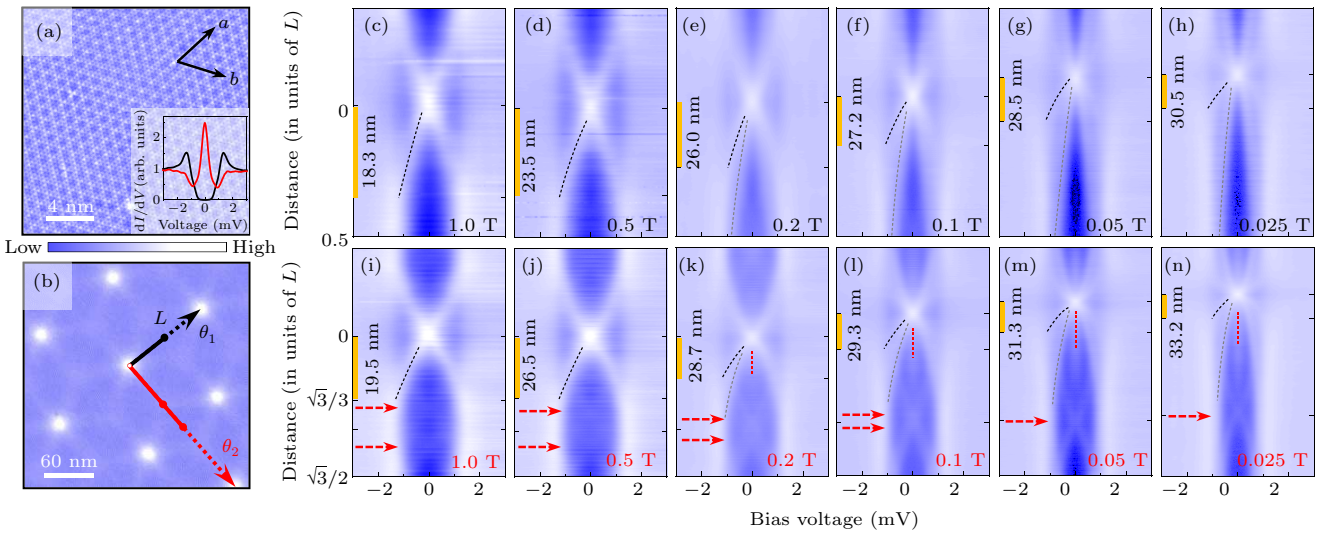



**Fig. 1.** (a) A $(20 \times 20)$-nm topographic STM image obtained at 1.6 K with the bias voltage of $-50$ mV and the feedback current of 50 pA. The primary vectors are labeled as $a$ and $b$. The inset displays the typical tunneling spectra at 0.45 K, the black curve denotes that obtained without a magnetic field, and the red one was measured at a vortex center under 200 mT. (b) ZBC map measured at 200 mT showing the spatial distribution of vortices. The black and red arrows indicate the nearest and next nearest neighboring directions labeled as $\theta_1$ and $\theta_2$, respectively. The dots on the arrows denote the special positions in between the neighboring vortices. STS conditions: $V_b = -4$ mV, $I_s = 0.1$ nA, lock-in modulation $V_m = 0.2$ mV. (c)–(h) False color maps of the spatially evolved $dI/dV$ spectra across a vortex center, along $\theta_1$ at 1 T, 500 mT, 200 mT, 100 mT, 50 mT, and 25 mT. Each vertical axis is calibrated in units of vortex spacing $L$. The black dashed lines show the extension trajectory of the outer branch, whose lengths are displayed by the orange line segments on the left. The gray dashed lines show the extension trajectory of the inner branch. STS conditions: $V_b = -4$ mV, $I_s = 0.8$ nA, $V_m = 0.1$ mV. (i)–(n) Evolved $dI/dV$ spectra along $\theta_2$ at 1 T, 500 mT, 200 mT, 100 mT, 50 mT, and 25 mT. The black and gray dashed lines denote the outer and inner branches, respectively. The red dashed line depicts a resolved non-splitting ZBCP. The red arrows indicate an LDOS enhancement near the center between three neighboring vortices. STS conditions: $V_b = -4$ mV, $I_s = 0.8$ nA, $V_m = 0.1$ mV.

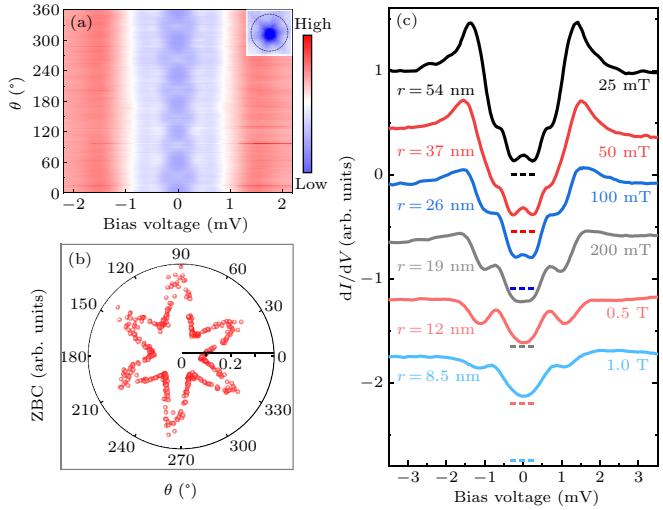



**Fig. 2.** (a) Angle-dependent evolution of the $dI/dV$ spectra along a circle 40 nm away from the vortex center. The inset shows a zero energy conductance map with a size of 97.5 nm $\times$ 97.5 nm at 25 mT, and the dashed circle represents trajectories with a radius of 40 nm. STS conditions: $V_b = -4$ mV, $I_s = 0.8$ nA, $V_m = 0.1$ mV. (b) Angle-dependent evolution of the ZBC extracted from (a), which are normalized by the $dI/dV$ value at $V_b$. (c) Tunneling spectra obtained at certain distances ($r/L = 0.17$) away from the vortex core center along the direction of $\theta_2$. STS conditions: $V_b = -4$ mV, $I_s = 0.8$ nA, $V_m = 0.1$ mV.

To clarify this issue, we measured the angle-dependent $dI/dV$ spectra along a circle 40 nm away from a vortex center at 25 mT as displayed in Fig. 2(a). The angular coordinate begins from $\theta = 0°$, which is defined as the atomic primary orientation $a$. Significantly, the non-splitting ZBCP appears periodically in the six-fold rotation symmetric directions of $\theta_2$. This is further verified by the periodically enhanced ZBCs in Fig. 2(b), which were extracted from the spectra in Fig. 2(a). Thus, the vortex bound states also host the six-fold symmetry but deflect 30° from the crystal structure and the vortex lattice, we can not determine the causation of the anisotropic ZBCP and the crossing features from either the vortex–vortex interactions[34] or the intrinsic FS or gap anisotropy.[29,30] These delicate features may be smeared out in finite magnetic fields or higher temperatures, which were rarely described in the previous studies on $NbSe_2$. To further verify the key effect of extremely low magnetic fields on revealing the detailed vortex bound states, we compared typical spectra along $\theta_2$ under varied fields in Fig. 2(c). The sharp coherence peaks and the vivid in-gap features become substantially obscured when the applied field exceeds 100 mT, though the field induced pair-breaking effect is not that intense. Hence, it is reasonable to speculate that the intervortex transfer of the quasiparticles

smears distinct features on the density of states, making a significant influence on the intrinsic vortex bound states.

In this sense, intrinsic vortex structures excluding vortex–vortex interactions are strongly desired to be revealed. With the temperature constant at 0.45 K, there is a certain probability of observing an isolated vortex by applying a magnetic field along the $c$ direction and then withdrawing the field. The trapped isolated vortex provides an excellent platform to shed light on this issue. Figure 3(a) displays the ZBC mapping of a trapped isolated vortex at 0 T, which exhibits intrinsically anisotropic characteristics with six rays extending along the directions of $\theta_2$ (shown by the red dash lines). This suggests that the anisotropic vortex bound states are rooted in the intrinsically anisotropic properties of $NbSe_2$ but not the neighboring vortices interactions. The LDOS along the $\theta_1$ direction in Fig. 3(b) shows similar evolution to those measured in the low fields, with a broad ZBCP in the vortex center splitting into two pairs of dispersive branches within our best resolution. For the evolution along the direction of $\theta_2$ shown in Fig. 3(c), there still exists the robust ZBCP character extending more than 100 nm away from the dispersive branches as indicated by the dash lines. It should be pointed out that, we failed to observe this anisotropic ZBCP at 1.6 K either in vortices under extremely low fields or a trapped isolated vortex at zero field, lacking robustness against the thermal excitations in addition to the vortex–vortex interactions. On the other hand, the above-mentioned small X-shaped crossing features along $\theta_2$ outside the vortex core are no longer visible. These results clearly show that the X-shaped crossing features arise from the vortex–vortex interaction while the anisotropic non-splitting ZBCP is an intrinsic feature of the vortex bound state of $NbSe_2$.

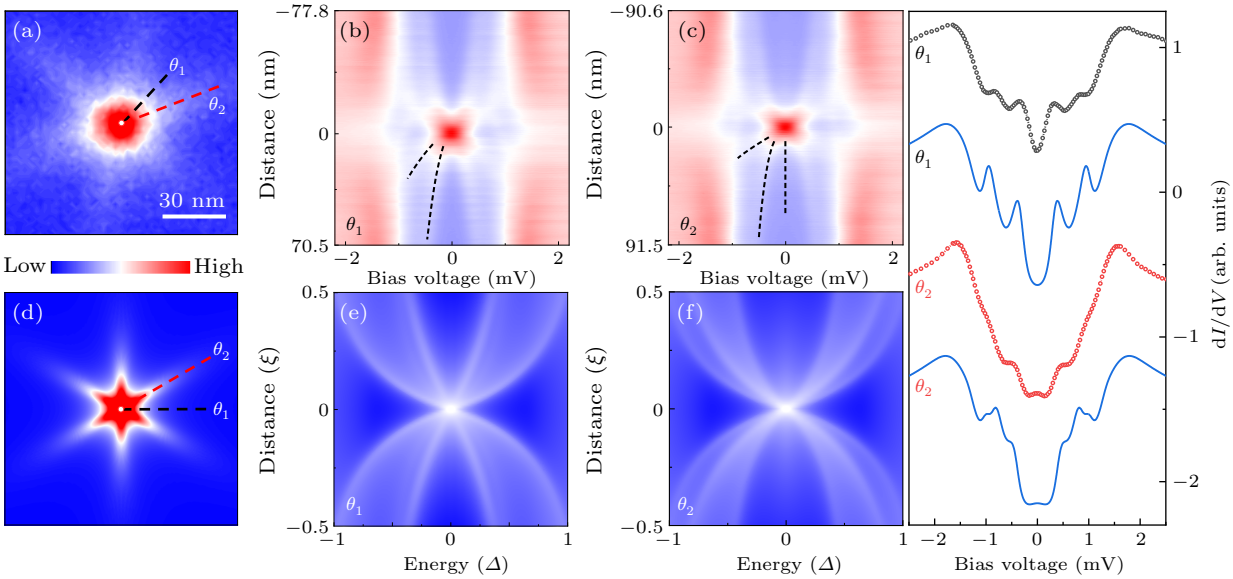



**Fig. 3.** (a) Zero-bias $dI/dV$ map around an isolated vortex at 0 T. STS conditions: $V_b = -4$ mV, $I_s = 0.1$ nA, $V_m = 0.2$ mV. (b) and (c) Color map of the spatially resolved $dI/dV$ spectra across the isolated vortex center along the directions of $\theta_1$ and $\theta_2$. (d) The calculated zero-energy LDOS map in a $1.0\xi \times 1.0\xi$ area for an isolated vortex. (e) and (f) Theoretically calculated spatial evolutions of the vortex bound states across an isolated vortex center along the directions of $\theta_1$ and $\theta_2$, respectively. (g) Comparison of experimental and theoretical typical spectra along the directions of $\theta_1$ and $\theta_2$, hollow dots represent experimental data and solid lines represent theoretical simulation data. For better comparison, theoretical data was subjected to a thermal broadening treatment of 0.45 K.

From this point of view, it has been theoretically explained that anisotropic vortex states can result from the intrinsic anisotropy of the FS or superconducting gaps.[28–30] The latter is known to be much more pronounced than the former in $NbSe_2$.[31,35,36] Unfortunately, the models were difficult to verify experimentally for lacking a truly isolated vortex in the past to the best of our knowledge. We simulated the LDOS of an isolated vortex with anisotropic gaps to compare with our results by using the quasi-classical Green function approach within the self-consistently obtained pair potential.[37] Figure 3(d) shows the calculated ZBC around the isolated vortex by using an anisotropic superconducting gap $\Delta(\theta) = \Delta_0[1 + (1/3)\cos(6\theta)]$, which reproduces the star-shaped vortex states. Figures 3(e) and 3(f) show the low energy LDOS along the two special directions $\theta_1$ and $\theta_2$, respectively. Besides, we extracted typical spectra from Figs. 3(b), 3(c), 3(e), and 3(f) for comparison as shown in Fig. 3(g). It can be seen that the discrete energy levels split into symmetric branches along the two characteristic directions, however, a unique anisotropic non-splitting ZBCP is formed only along the $\theta_2$ direction, showing good agreement with our experimental observations. This suggests that the anisotropic non-splitting ZBCP of $NbSe_2$ stems from the anisotropy of the superconducting gap, while the vortex–vortex interactions also produce an essential impact on the performance of the vortex bound states. There is still a slight difference between theo-

retical simulation and experiment. To completely reproduce the performance of theoretical calculations, lower temperature and higher energy resolutions are required. Due to their topologically trivial electronic structure, these results call for caution when interpreting spatially non-splitting ZBCP in vortex cores as an essential signature of MZMs in superconductors with anisotropic gaps or FS far from the quantum limit.

Since the vortex bound states are sensitive to the magnetic field, it is meaningful to determine the vortex core size $\xi_c$ towards the zero-field limit. The vortex core size is defined as $\xi_c = \Delta_0[\mathrm{d}\Delta(r)/\mathrm{d}r|_{r\to 0}]^{-1}$, which is usually obtained by fitting the evolution of the normalized ZBC across the vortex center to evaluate the superconducting coherence length.[38,39] An accurate model with convergence condition $\mathrm{d}\Delta(r)/\mathrm{d}r|_{r\to L/2} = 0$ for the two-band system was adopted to determine the value of $\xi_c$, which takes the periodicity of the vortex lattice into account.[40,41]

$$\sigma = 1 - \frac{\delta_1^2(x) + \gamma\delta_2^2(x)}{\delta_1^2(1) + \gamma\delta_2^2(1)}, \quad \gamma = \frac{n_2}{n_1},$$
$$\delta_\nu = \frac{x}{\sqrt{(x^2+\eta_\nu^2)}} \exp\left(-\frac{x^2\eta_\nu^2}{2(1+\eta_\nu^2)}\right),$$

where $x = 2r/L$, $\eta_\nu = 2\xi_{c\nu}/L$, $\nu = 1, 2$, and $L$ is the nearest neighbor spacing of vortices. We have performed this analysis to extract the field-dependent $\xi_c$ by fitting the ZBC profiles across the vortex center along the $\theta_1$ direction, avoiding the influence of the zero energy anomalies along $\theta_2$. Figures 4(a) and 4(b) display the double-coordinate normalized experimental ZBC data for $T = 0.45$ K and 1.6 K, respectively. It can be directly observed that as the magnetic fields increase, the individual vortex gradually expands in the Wigner–Seitz unit cell of the vortex lattice, resulting in enhanced interactions between each other. This is also the primary factor contributing to the formation of a hexagonal vortex lattice in the absence of a strong pinning effect. We find that the data can be well described with the same $\xi_c$ for two bands as demonstrated by the corresponding best-fitting curves, which is consistent with the behavior of multiband superconductors $NbSe_{1.8}S_{0.2}$, $NbS_2$ and $CaKFe_4As_4$.[40,41] Recently, theoretical considerations re-examine the almost identical vortex core sizes in two-band superconductors with a microscopic approach that covers a broad temperature and magnetic field regime.[42] Such a behavior which is also known as "length-scales locking" is a robust phenomenon for a moderately coupled multiband system.

To definitively confirm this and eliminate any influence from vortex–vortex interactions, it is preferable to determine the intrinsic vortex core size based on a single trapped vortex in the absence of external fields. In this case, the intervortex spacing $L$ used in the model should ideally be infinite. We have concluded that $\xi_c$s converge when the intervortex spacing $L$ is taken to be sufficiently large during the fitting process for the isolated vortex. Figure 4(c) presents the ZBC profiles of the isolated single vortex with the fitted curves superposed on them for temperatures of 0.45 K and 1.6 K, respectively. Remarkably, the fittings using the same $\xi_c$ still exhibit excellent agreement with the experimental data, implying a not weak interband coupling in this system.[42,43] We could finally define the vortex core sizes in the zero-field limit based on the same model. Upon initial inspection, the size of the isolated single vortex at 1.6 K is much larger than that at 0.45 K, in spite of the little superconducting gap variation deduced from the Bardeen–Cooper–Schrieffer relationship.[44] This thermal excited expansion, known as the Kramer–Pesch effect, can be attributed to the increased population of the in-gap quasiparticle states with larger wave function radii.[45]

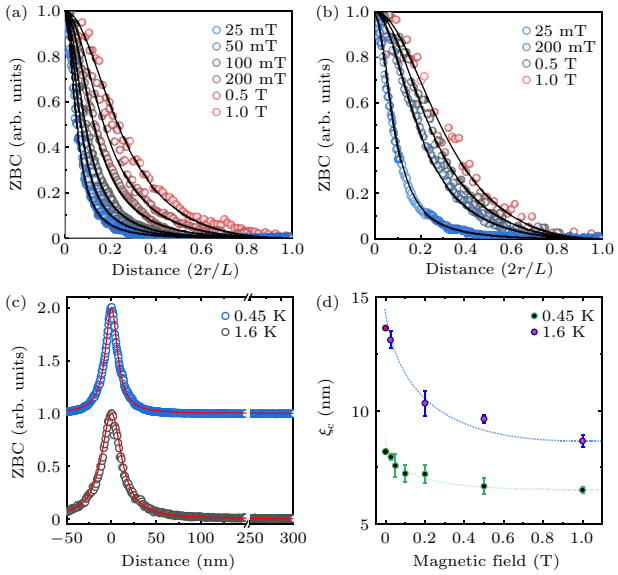



**Fig. 4.** (a) and (b) Normalized ZBC measured across vortex center under a series of fields at 0.45 K and 1.6 K with the fitting results. (c) Normalized ZBC measured across an isolated vortex under zero fields at 0.45 K and 1.6 K, in addition to the fitting results. (d) The relationship between vortex core size $\xi_{c1,2}$ and magnetic fields, and different colored points represent different bands. The lines are for guides. STM conditions are the same in panels (a)–(c): $V_b = -4$ mV, $I_s = 0.8$ nA, $V_m = 0.1$ mV.

Moreover, the $\xi_c$ values of the trapped single vortex are respectively larger than those of any other vortices in finite fields at the same temperature. In clean superconductors, the shrinkage of the vortex core with the increasing magnetic field at low temperatures can be attributed to two key factors related to vortex–vortex interactions. The first one is the vortex lattice squeezing effect, which arises from the overlap of the superfluid surrounding the vortex cores, particularly the cancellation of opposite supercurrents between the adjacent vortices. This overlap significantly alters the overall distribution of $\boldsymbol{j}_s(\boldsymbol{r})$, and then modifies $B(\boldsymbol{r})$ and $\Delta(\boldsymbol{r})$.[22] The second factor is the quasiparticle delocalization effect induced by the quasiparticle transfer between the neighboring vortices due to the wavefunction hybridization of their in-gap bound

states.[24–26] $\xi_c$s show a decrease at the extremely low fields and then the weak field dependence at 0.45 K as guided by the green curve. The vortex core size behaviors we obtained from the density of states are relatively consistent with that obtained from the μSR experiment by fitting $B(r)$.[22] In the μSR experiment, this non-monotonic behavior is attributed to the different quasiparticle localization effects of the different gaps.[22,46–48] However, this behavior of the vortex core sizes is consistent with that predicted by theory for multiband systems with "length-scales locking".[42] As a side note, such measurement is difficult to achieve through other methods in the zero-field limit, highlighting the unique role played by STM on the trapped single vortex at 0 T. Furthermore, the trapped vortices could be artificially enhanced by introducing defects or adatoms as the pinning centers into various superconducting systems.[49–54]

## 4. Conclusion

In conclusion, we revisited the fine structure of the vortex states of 2H-$NbSe_2$ under extremely low magnetic fields towards zero fields by low-temperature scanning tunneling microscope. Some anisotropic fine structures were revealed on the evolving spectra across the vortex center along the next nearest neighboring direction, including some crossing features and spatially extended zero bias peak. Based on the results around a trapped isolated vortex without any external magnetic field, these features were respectively identified as the effect of the vortex–vortex interactions and the intrinsic superconducting gap anisotropy. Furthermore, we showed the relationship between vortex core size and magnetic fields at different temperatures, which contains vortex core size under the zero-field limit. It provides an effective way to determine the vortex states at the zero-field limit, which could be widely used for many type-Ⅱ superconductors.

## Acknowledgments

We are grateful to Prof. Y. Nagai for stimulating discussions. Project supported by the National Key R&D Program of China (Grant No. 2022YFA1403203), the Innovation Program for Quantum Science and Technology (Grant No. 2021ZD0302802), the National Natural Science Foundation of China (Grant Nos. 12074002, 12374133, and 11804379), and the Major Basic Program of Natural Science Foundation of Shandong Province (Grant No. ZR2021ZD01). Y. J. acknowledges the supports of the National Natural Science Foundation of China (Grant No. 12274001) and the Natural Science Foundation of Anhui Province (Grant No. 2208085MA09).

## References

[1] Abrikosov A A 1957 *Soviet Physics-JETP* **5** 1174
[2] Gor'kov L 1959 *Zh. Exsper. Teoret. Fiz* **36** 1918
[3] Caroli C, De Gennes P and Matricon J 1964 *Physics Letters* **9** 307
[4] Hayashi N, Isoshima T, Ichioka M and Machida K 1998 *Phys. Rev. Lett.* **80** 2921
[5] Gygi F m c and Schlüter M 1991 *Phys. Rev. B* **43** 7609
[6] Nayak C, Simon S H, Stern A, Freedman M and Das Sarma S 2008 *Rev. Mod. Phys.* **80** 1083
[7] Sato M and Ando Y 2017 *Reports on Progress in Physics* **80** 076501
[8] Kong L, Zhu S, Papaj M, Chen H, Cao L, Isobe H, Xing Y, Liu W, Wang D, Fan P, Sun Y, Du S, Schneeloch J, Zhong R, Gu G, Fu L, Gao H J and Ding H 2019 *Nat. Phys.* **15** 1181
[9] Fu L and Kane C L 2008 *Phys. Rev. Lett.* **100** 096407
[10] Xu J P, Wang M X, Liu Z L, Ge J F, Yang X, Liu C, Xu Z A, Guan D, Gao C L, Qian D, Liu Y, Wang Q H, Zhang F C, Xue Q K and Jia J F 2015 *Phys. Rev. Lett.* **114** 017001
[11] Wang D, Kong L, Fan P, Chen H, Zhu S, Liu W, Cao L, Sun Y, Du S, Schneeloch J, Zhong R, Gu G, Fu L, Ding H and Gao H J 2018 *Science* **362** 333
[12] Wang Z, Rodriguez J O, Jiao L, Howard S, Graham M, Gu G D, Hughes T L, Morr D K and Madhavan V 2020 *Science* **367** 104
[13] Li M, Li G, Cao L, Zhou X, Wang X, Jin C, Chiu C K, Pennycook S J, Wang Z and Gao H J 2022 *Nature* **606** 890
[14] Liu Q, Chen C, Zhang T, Peng R, Yan Y J, Wen C H P, Lou X, Huang Y L, Tian J P, Dong X L, Wang G W, Bao W C, Wang Q H, Yin Z P, Zhao Z X and Feng D L 2018 *Phys. Rev. X* **8** 041056
[15] Guan S Y, Chen P J, Chu M W, Sankar R, Chou F, Jeng H T, Chang C S and Chuang T M 2016 *Science Advances* **2** e1600894
[16] Liang Z, Hou X, Zhang F, Ma W, Wu P, Zhang Z, Yu F, Ying J J, Jiang K, Shan L, Wang Z and Chen X H 2021 *Phys. Rev. X* **11** 031026
[17] Suderow H, Guillamón I, Rodrigo J G and Vieira S 2014 *Superconductor Science and Technology* **27** 063001
[18] Fischer O, Kugler M, Maggio-Aprile I, Berthod C and Renner C 2007 *Rev. Mod. Phys.* **79** 353
[19] Hoffman J E 2011 *Reports on Progress in Physics* **74** 124513
[20] Yin J X, Pan S H and Zahid Hasan M 2021 *Nature Reviews Physics* **3** 249
[21] Liu X, Chong Y X, Sharma R and Davis J C S 2021 *Nat. Mater.* **20** 1480
[22] Callaghan F D, Laulajainen M, Kaiser C V and Sonier J E 2005 *Phys. Rev. Lett.* **95** 197001
[23] Sonier J E 2004 *J. Phys.: Condens. Matter* **16** S4499
[24] Pöttinger B and Klein U 1993 *Phys. Rev. Lett.* **70** 2806
[25] Ichioka M, Hasegawa A and Machida K 1999 *Phys. Rev. B* **59** 184
[26] Canel E 1965 *Physics Letters* **16** 101
[27] Machida T, Sun Y, Pyon S, Takeda S, Kohsaka Y, Hanaguri T, Sasagawa T and Tamegai T 2019 *Nat. Mater.* **18** 811
[28] Kim H, Nagai Y, Rózsa L, Schreyer D and Wiesendanger R 2021 *Applied Physics Reviews* **8** 031417
[29] Hayashi N, Ichioka M and Machida K 1996 *Phys. Rev. Lett.* **77** 4074
[30] Nagai Y, Ueno Y, Kato Y and Hayashi N 2006 *J. Phys. Soc. Jpn.* **75** 104701
[31] Rahn D J, Hellmann S, Kalläne M, Sohrt C, Kim T K, Kipp L and Rossnagel K 2012 *Phys. Rev. B* **85** 224532
[32] Hess H F, Robinson R B and Waszczak J V 1990 *Phys. Rev. Lett.* **64** 2711
[33] Dalrymple B, Mroczkowski S and Prober D 1986 *Journal of Crystal Growth* **74** 575
[34] Ichioka M, Hayashi N and Machida K 1997 *Phys. Rev. B* **55** 6565
[35] Sanna A, Pellegrini C, Liebhaber E, Rossnagel K, Franke K J and Gross E K U 2022 *npj Quantum Materials* **7** 6
[36] Galvis J A, Herrera E, Berthod C, Vieira S, Guillamón I and Suderow H 2018 *Communications Physics* **1** 30
[37] Hayashi N, Ichioka M and Machida K 1997 *Phys. Rev. B* **56** 9052
[38] Eskildsen M R, Kugler M, Tanaka S, Jun J, Kazakov S M, Karpinski J and Fischer O 2002 *Phys. Rev. Lett.* **89** 187003
[39] Xu J P, Liu C, Wang M X, Ge J, Liu Z L, Yang X, Chen Y, Liu Y, Xu Z A, Gao C L, Qian D, Zhang F C and Jia J F 2014 *Phys. Rev. Lett.* **112** 217001
[40] Fente A, Herrera E, Guillamón I, Suderow H, Mañas Valero S, Galbiati M, Coronado E and Kogan V G 2016 *Phys. Rev. B* **94** 014517
[41] Fente A, Meier W R, Kong T, Kogan V G, Bud'ko S L, Canfield P C, Guillamón I and Suderow H 2018 *Phys. Rev. B* **97** 134501

[42] Ichioka M, Kogan V G and Schmalian J 2017 *Phys. Rev. B* **95** 064512
[43] Noat Y, Silva-Guillén J A, Cren T, Cherkez V, Brun C, Pons S, Debontridder F, Roditchev D, Sacks W, Cario L, Ordejón P, García A and Canadell E 2015 *Phys. Rev. B* **92** 134510
[44] Bardeen J, Cooper L N and Schrieffer J R 1957 *Phys. Rev.* **108** 1175
[45] Kramer L and Pesch W 1974 *Zeitschrift für Physik* **269** 59
[46] Ichioka M, Machida K, Nakai N and Miranović P 2004 *Phys. Rev. B* **70** 144508
[47] Nakai N, Ichioka M and Machida K 2002 *J. Phys. Soc. Jpn.* **71** 23
[48] Boaknin E, Tanatar M A, Paglione J, Hawthorn D, Ronning F, Hill R W, Sutherland M, Taillefer L, Sonier J, Hayden S M and Brill J W 2003 *Phys. Rev. Lett.* **90** 117003
[49] Cho K, Kończykowski M, Teknowijoyo S, Tanatar M A, Guss J, Gartin P B, Wilde J M, Kreyssig A, McQueeney R J, Goldman A I, Mishra V, Hirschfeld P J and Prozorov R 2018 *Nat. Commun.* **9** 2796
[50] Zhang S S, Yin J X, Dai G, Zhao L, Chang T R, *et al.* 2020 *Phys. Rev. B* **101** 100507
[51] Fasano Y, Herbsommer J A, de la Cruz F, Pardo F, Gammel P L, Bucher E and Bishop D J 1999 *Phys. Rev. B* **60** R15047
[52] Fasano Y and Menghini M 2008 *Superconductor Science and Technology* **21** 023001
[53] Chen X H, Dai P C, Feng D L, Xiang T and Zhang F C 2014 *National Science Review* **1** 371
[54] Gu Q Q and Wen H H 2022 *The Innovation* **3** 100202